Bistatic Transfer Function for a Planar Distribution of Stationary Scatterers: Analytical Results

Octavio Cabrera and Damián H. Zanette

***Abstract*—We present exact and approximate analytical results for signal transmission through a planar distribution of stationary scatterers in a bistatic configuration. The transfer function of this transmission channel is computed by assuming a continuous cross-section density. This approach makes it possible to obtain explicit mathematical expressions for a wide variety of scatterer distributions. The inverse problem, where the scatterer distribution is inferred from the transfer function, is also considered. Analytical results are compared with numerical simulations for randomly distributed point scatterers, using real-life FM signals. Transfer functions for these stylized scatterer distributions may provide a base for more realistic mathematical models of the environment.**

***Index Terms*—Bistatic radar, channel models, transfer function.**

I. Introduction

BISTATIC configurations, with noncollocated emitter and receiver, are the basic working setup of a class of radar systems with increasing impact in remote sensing, such as synthetic aperture radars (SAR) and passive radars [1]. Presently, SAR is the leading technique for radar terrain imaging from aircraft and satellites, with applications that range from elevation mapping based on interferometry to polarimetric soil identification. Very recent SAR developments in geosciences have included the measurement of oceanic currents [2], terrain movement detection [3], and the design on multiple-input and multiple-output quasi-geostationary systems [4]. Physical separation between the emitter and the receiver enhances the information content of SAR data, thus improving feature detection and characterization [5]. Passive radars, in turn, are intrinsically bistatic systems, since any noncooperative source illuminating the environment is typically located some distance away from the user's receiving antenna [6]. Exploiting noncooperative sources for remote sensing is a promising possibility for expanding the use of low-cost radars over a broad variety of applications.

Sensing systems, such as SAR and passive radars, are based on the inference of environmental features from a comparison between the emitted and the received signals. The environment acts as a transmission channel from the emitter to the receiver, modifying the emitted signal by the addition of echoes generated from reflection in material objects, and by attenuation during propagation. Processing of the received signal thus makes it possible to extract information on the location of scatterers and on their motion and, to a certain extent, on their nature. Generally, the interpretation of this information requires possessing in advance a model for the distribution and dynamics of the scatterers, and for their interaction with electromagnetic radiation. The construction of such models is a central chapter of radar signal processing, and this is often based on a combination of empirical and heuristic arguments. Rayleigh, Weibull, and lognormal statistical cross-section distributions [7], and Okamura and Hata path-loss models [8], are just a few standard examples belonging to this kind of approach.

In this letter, we present mathematical results on the characterization of the received signal in a bistatic radar, for a wide class of stationary scatterer distributions. Our formulation is based on the computation of the transfer function, which is defined as the ratio between the signals measured at the positions of the receiver and the emitter, which are both expressed in the frequency domain. In Section II, we find an integral form for the transfer function of a planar distribution of scatterers. This distribution is approximated by a continuous function, and the positions of the receiver and the emitter are assumed to be coplanar with the scatterers. The inverse problem, namely, finding the scatterer distribution from the transfer function, is also considered. Then, the transfer function is exactly calculated as a function of the frequency for a variety of scatterer distributions, and a general approximation for high frequencies is obtained. In Section III, analytical results are compared with numerical simulations, using real-life signals and randomly distributed point scatterers.

Our mathematical problem is set up as an approximation to a bistatic radar system, whose two antennas are situated near the surface of Earth, with signal echoes generated at, or close to, the surface itself. However, the highly stylized scatterer distributions considered in the calculation make it clear that the results are not expected to give an accurate description of specific realistic situations. Instead, they have to be regarded as a well-founded starting point on which more sophisticated models can be built up. On the other hand, our first-principle approach overcomes the heuristic nature of the standard models referred to earlier. Moreover, since our characterization of the scattering channel preserves full information about the transmitted signal's amplitude and phase, the present method can be adapted to evaluate a host of quantities of interest in radar signal processing, wireless communication, and interferometry, among others.

Manuscript received May 18, 2015; revised July 29, 2015; accepted August 29, 2015. Date of publication September 23, 2015; date of current version October 27, 2015. The works of O. Cabrera and D. H. Zanette are supported by the Consejo Nacional de Investigaciones Científicas y Técnicas (CONICET), Argentina.

The authors are with the Centro Atómico Bariloche and Instituto Balseiro (CNEA and UNCuyo), 8400 San Carlos de Bariloche, Argentina (e-mail: cabreraoct@gmail.com; zanette@cab.cnea.gov.ar).

Color versions of one or more of the figures in this paper are available online at http://ieeexplore.ieee.org.

Digital Object Identifier 10.1109/LGRS.2015.2475635

II. Bistatic Transfer Function for Continuously Distributed Scatterers

Let $\mathbf{r}_E$ and $\mathbf{r}_R$ be the positions of the emitter and the receiver, respectively. We assume that the signal propagates in free space, and it is reflected by a set of N stationary scatterers situated at positions $\mathbf{r}_k$, with cross sections $\sigma_k (k = 1, \ldots, N)$, independent of frequency and polarization. If the amplitude of the emitted (real) signal is $E(t)$, at the receiver's position we have

$$R(t) = \frac{1}{d_0} E(t - T_0) + \sum_{k=1}^{N} \frac{\sqrt{\sigma_k}}{d_E^{(k)} d_R^{(k)}} E(t - T_k) \qquad (1)$$

where $d_0 = |\mathbf{r}_R - \mathbf{r}_E|$ is the distance between the emitter and the receiver; $T_0 = d_0/c$ is the corresponding time delay; $d_E^{(k)} = |\mathbf{r}_k - \mathbf{r}_E|$ and $d_R^{(k)} = |\mathbf{r}_k - \mathbf{r}_R|$ are the distances from the kth scatterer to the emitter and the receiver, respectively; and $T_k = (d_E^{(k)} + d_R^{(k)})/c$ is the total delay of the echo received from that scatterer. In the frequency domain, (1) reads

$$\tilde{R}(\omega) = \frac{1}{d_0} \tilde{E}(\omega) \left[1 + \tau(\omega)\right] e^{-j\omega d_0/c} \qquad (2)$$

where

$$\tau(\omega) = d_0 e^{j\omega d_0/c} \sum_{k=1}^{N} \frac{\sqrt{\sigma_k}}{d_E^{(k)} d_R^{(k)}} e^{-j\omega \left(d_E^{(k)} + d_R^{(k)}\right)/c}$$

is the transfer function associated with the scattering channel. According to this definition, $\tau(\omega)$ stands for the (complex) ratio between the signal received through the scattering channel and the direct emitter–receiver signal.

We assume that the positions $\mathbf{r}_k$ of the scatterers, as well as those of the emitter and receiver, i.e., $\mathbf{r}_E$ and $\mathbf{r}_R$, are all coplanar. Suppose, moreover, that the distribution of scatterers over the plane is well represented by a function $n(\mathbf{r}, \sigma)$, where the product $n(\mathbf{r}, \sigma) d^2\mathbf{r}\, d\sigma$ gives the (infinitesimal) number of scatterers in the surface element $d^2\mathbf{r}$, with cross section in the interval $(\sigma, \sigma + d\sigma)$. In terms of $n(\mathbf{r}, \sigma)$, the transfer function can be expressed in integral form as

$$\tau(\omega) = d_0 e^{j\omega d_0/c} \int \frac{\rho(\mathbf{r})\, e^{-j\omega(|\mathbf{r}-\mathbf{r}_E| + |\mathbf{r}-\mathbf{r}_R|)/c}}{|\mathbf{r} - \mathbf{r}_E||\mathbf{r} - \mathbf{r}_R|} d^2\mathbf{r} \qquad (3)$$

where $\rho(\mathbf{r}) = \int_0^\infty n(\mathbf{r}, \sigma) \sqrt{\sigma}\, d\sigma$ is the local mean value of $\sqrt{\sigma}$ at position $\mathbf{r}$. This function is to be interpreted as the spatial distribution of scatterers weighted by the square root of their respective cross sections. If the positions and the cross sections of the scatterers are statistically uncorrelated, the function $n(\mathbf{r}, \sigma)$ factorizes as $n(\mathbf{r}, \sigma) = \rho(\mathbf{r}) S(\sigma) / \langle\sqrt{\sigma}\rangle$, with $\langle\sqrt{\sigma}\rangle = \int_0^\infty \sqrt{\sigma} S(\sigma)\, d\sigma$.

The integral in (3) is related to the Fresnel–Kirchhoff integrals of the scalar diffraction theory [9]. It takes a particularly simple form if expressed in elliptic coordinates μ and ν, with foci at the emitter and the receiver. Elliptic coordinates [10] and the standard Cartesian coordinates x and y are linked through the equations $x = x_0 \cosh\mu \cos\nu$ and $y = x_0 \sinh\mu \sin\nu$, where $x_0 = d_0/2$ is half the distance between the two foci. The coordinates μ and ν take values in the intervals $0 \le \mu < \infty$ and $0 \le \nu < 2\pi$. Ellipses and hyperbolas in Fig. 1 respectively correspond to the curves of constant μ and ν, which

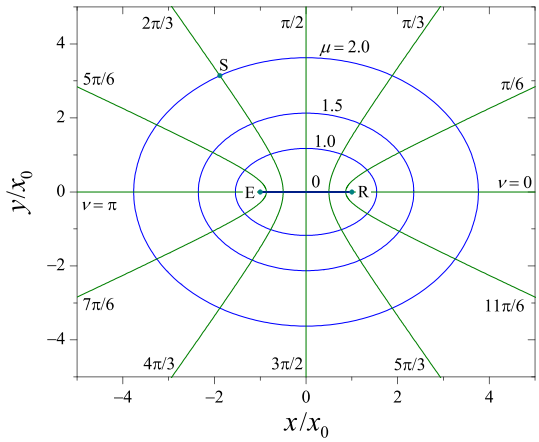

Fig. 1. Ellipses and hyperbolas represent, respectively, the curves of constant μ and ν in the elliptic coordinate system described in the text, which are plotted on the Cartesian plane. Dots stand for the positions of the emitter (E) and the receiver (R), which coincide with the two foci common to all ellipses, and of a generic scatterer (S) with $\mu = 2$ and $\nu = 2\pi/3$.

are plotted on the Cartesian plane with the coordinates x and y scaled by the distance x_0. In terms of μ and ν, (3) becomes

$$\tau(\omega) = d_0 \int_0^\infty \bar{\rho}(\mu)\, e^{j\frac{\omega d_0}{c}(1 - \cosh\mu)} d\mu \qquad (4)$$

where the marginal distribution $\bar{\rho}(\mu) = \int_0^{2\pi} \rho(\mathbf{r})\, d\nu$ defines the number of scatterers (weighted by $\sqrt{\sigma}$) over the ellipse of "modulus" μ, given by the product $\bar{\rho}(\mu)\, d\mu$. We see that the detailed dependence of $\rho(\mathbf{r})$ on the "angle" ν is irrelevant to the form of $\tau(\omega)$. This is a consequence of the fact that time delays in the echoes from scatterers on any given ellipse are identical to each other. Equation (4) shows, moreover, that $\tau(\omega)$ depends on the frequency through the nondimensional parameter $w = \omega d_0/c$ only.

Using suitable variable changes and elementary properties of the Fourier transform, the integral relation between the transfer function and the marginal distribution $\bar{\rho}(\mu)$ can be inverted as

$$\bar{\rho}(\mu) = \frac{\sinh\mu}{2\pi c} \int_{-\infty}^{\infty} \tau(\omega)\, e^{-j\frac{\omega d_0}{c}(1 - \cosh\mu)} d\omega. \qquad (5)$$

This expression makes it possible to infer information on the distribution of scatterers if the transfer function is known, for instance, from measurements.

A. Exact Results for $\tau(\omega)$

The integral in (4) can be exactly calculated for a few significant choices of the marginal scatterer distribution $\bar{\rho}(\mu)$. A convenient change of variables to manipulate the integral is $u \equiv \cosh\mu$, with $d\mu = (u^2 - 1)^{-1/2} du$, which converts the calculation into an integral similar to a Fourier transform. The results presented in what follows are valid for $\omega > 0$. The transfer function for $\omega < 0$ can be readily obtained from the identity $\tau(-\omega) = \tau^*(\omega)$, where the asterisk indicates the complex conjugate.

The simplest case corresponds to a constant distribution, i.e., $\bar{\rho}(\mu) = \rho_0$. Although this choice describes the rather unrealistic situation where the received signal contains contributions from

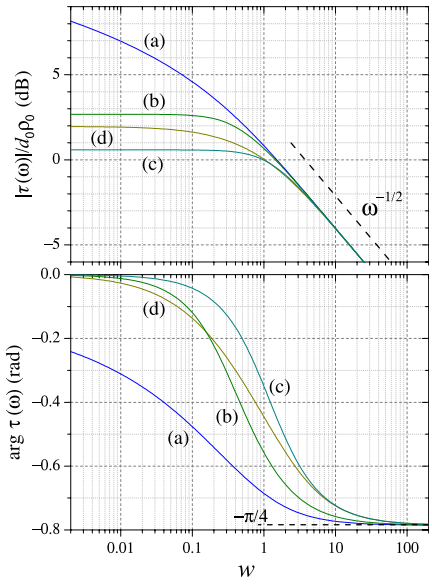

Fig. 2. Bode diagram of the transfer functions obtained in Section II-A, for four scatterer distributions: (a) uniform; (b) exponential, with $\alpha = 0.3$; (c) exponential, with $\alpha = 1.0$; (d) algebraic. Note that the horizontal axis stands for the nondimensional frequency $w = \omega d_0/c$, while in the vertical axis of the uppermost plot the transfer function is normalized by $d_0\rho_0$.

uniformly distributed and arbitrarily distant scatterers, it plays an important role for comparison with other cases. The transfer function is given by

$$\tau(\omega) = d_0\rho_0\, e^{jw} K_0(jw) \tag{6}$$

where $K_0(z)$ is the zeroth-order modified Bessel function of the second kind [10], and $w = \omega d_0/c$. The curves labeled by (a) on the Bode diagram in Fig. 2 stand for this result.

An immediate extension of the previous case is $\bar{\rho}(\mu) = \rho_0 \exp[\alpha(1-\cosh\mu)]$ with $\alpha > 0$, which reduces to the uniform distribution for $\alpha \to 0$. This choice of $\bar{\rho}(\mu)$ is obtained from a distribution of scatterers that decays exponentially with the distance to the emitter and the receiver. In Cartesian coordinates, it behaves as $\rho(\mathbf{r}) \sim \exp(-2\alpha\sqrt{x^2+y^2}/d_0)$ for large distances. The corresponding transfer function is given by

$$\tau(\omega) = d_0\rho_0\, e^{\alpha+jw} K_0(\alpha+jw). \tag{7}$$

The curves labeled by (b) and (c) in Fig. 2 stand for this result for $\alpha = 0.3$ and 1.0, respectively.

A third instance that results in an exact expression for $\tau(\omega)$ corresponds to $\bar{\rho}(\mu) = \rho_0/\cosh\mu$. In this case, the distribution of scatterers decays algebraically for large distances: $\rho(\mathbf{r}) \sim d_0/\sqrt{x^2+y^2}$. The decay is therefore slower than in the exponential case. The transfer function is now given by

$$\tau(\omega) = \frac{\pi}{2}\, d_0\rho_0\, e^{jw}\left[1 + \mathcal{K}_{(1,0)}(w) - j\mathcal{K}_{(0,-1)}(w)\right] \tag{8}$$

where we have defined $\mathcal{K}_{(p,q)}(w) = wK_p(jw)\mathbf{H}_q(w)$, with $K_p(z)$ and $\mathbf{H}_q(z)$ the Bessel and Struve functions, respectively [10]. The curves labeled by (d) in Fig. 2 stand for this result.

The results shown in Fig. 2 make it clear that the three cases considered earlier share the same behavior for large frequencies. In all of them, $|\tau(\omega)|$ decays as $\omega^{-1/2}$, while the argument of the transfer function asymptotically approaches $-\pi/4$. The limit of large frequencies, which is particularly relevant to applications, is studied in detail in Section II-B. For $\omega \to 0$, on the other hand, differences are especially important between the uniform distribution (a) and the other instances (b)–(d). In the former, $|\tau(\omega)| \sim -\ln\omega$, which diverges in the limit of small frequencies. In the latter, in contrast, $|\tau(\omega)|$ approaches constant values. The argument, in turn, tends to zero from below in all cases. In the uniform distribution, however, the approach is logarithmic, while in the other cases, we find a much faster algebraic approach.

B. Limit of Large Frequencies

For frequencies above a few hundred kilohertz and emitter–receiver distances on the order of the kilometers or larger, as expected to be the case in most applications of bistatic configurations, the nondimensional parameter $w = \omega d_0/c$ takes values around or above 10. At these values of w, unless the factor $1-\cosh\mu$ in the exponent of (4) is small, the exponential in the integrand is a rapidly oscillating function, whose positive and negative contributions compensate each other. Consequently, the integral is dominated by the interval of values of μ for which $\cosh\mu \approx 1$, i.e., for small μ. Within this interval, the factor in the exponent can be very well approximated by its first nonzero term in the Taylor series, as $1-\cosh\mu \approx -\mu^2/2$. Thus, we obtain the following approximation for the transfer function at large frequencies:

$$\tau(\omega) \approx d_0 \int_0^\infty \bar{\rho}(\mu)\, e^{-jw\mu^2/2} d\mu. \tag{9}$$

This approximation has the advantage that the collection of functions $\bar{\rho}(\mu)$ for which the integral can be explicitly calculated is broader than for (4). Note also that, although (9) is an approximation for large frequencies, it yields the exact value of $\tau(\omega)$, for $\omega = 0$. In practice, thus, the ranges where (9) gives an acceptable approximation to the exact transfer function might cover both large and small frequencies. An illustration of this situation is provided in Section III.

Before considering explicit results from (9), let us point out that, in the same spirit of the approximation for $1-\cosh\mu$, the distribution $\bar{\rho}(\mu)$ can be expanded as $\bar{\rho}(\mu) = \sum_{n=0}^{\infty} \rho_n \mu^n/n!$, when the derivatives $\rho_n = d^n\bar{\rho}/d\mu^n|_{\mu=0}$ exist for all orders. The integral in (9) can be obtained for each term in the Taylor series. The crudest approximation, given by the term with $n=0$, is $\tau(\omega) \approx \sqrt{\pi/2}\, d_0\rho_0\, w^{-1/2} \exp(-j\pi/4)$. This is the large-$\omega$ asymptotic behavior of all cases displayed in Fig. 2. The first correction to this asymptotic behavior is a purely imaginary contribution of order ω^{-1}, whose sign depends on the sign of ρ_1, i.e., on whether $\bar{\rho}(\mu)$ grows or decreases as $\mu \to 0$. If $\rho_1 = 0$ and $\rho_2 \neq 0$, the first significant correction is of order $\omega^{-3/2}$, and it depends on the convexity of $\bar{\rho}(\mu)$ at $\mu = 0$.

Equation (9) can be used to get simplified approximated forms for the transfer functions obtained in Section II-A. For the exponential distribution, for instance, we have $\bar{\rho}(\mu) = \rho_0 \exp[\alpha(1-\cosh\mu)] \approx \rho_0 \exp(-\alpha\mu^2/2)$. Inserted into (9), this yields $\tau(\omega) \approx d_0\rho_0\sqrt{\pi/2}(\alpha+jw)^{-1/2}$. For sufficiently large values of α, when the scatterers are concentrated in the low-μ zone, this is an excellent approximation to the exact result.

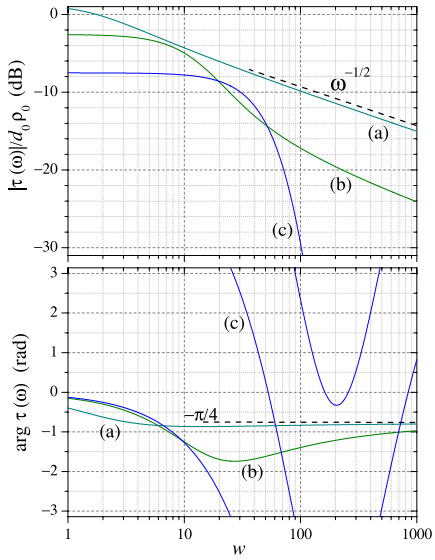

Fig. 3. Bode diagram of the large-ω transfer function for a Gaussian cluster of scatterers, i.e., $\bar{\rho}(\mu) = \rho_0 \exp[-a(\mu - \mu_0)^2]$, with $\mu_0 = 0.5$ and three values of a: (a) $a = 1$, (b) $a = 10$, and (c) $a = 100$. Note that the vertical axis in the lower panel spans the whole interval $(-\pi, \pi)$.

Among the distributions that admit an explicit treatment within the approximation of (9), a relevant instance is that of a localized cluster of scatterers. We consider first a cluster centered at the midpoint between emitter and receiver, i.e., $\rho(\mathbf{r}) \sim \exp[-(x^2 + y^2)/2s^2]$, for which we have chosen a Gaussian profile with standard deviation s. In the variable μ, this is equivalent to $\bar{\rho}(\mu) = \rho_0 \exp[a(1 - \cosh^2 \mu)] \approx \rho_0 \exp(-a\mu^2)$, where the coefficient $a = d_0^2/2s^2$ is inversely proportional to the Gaussian width squared. Within this approximation, thus, this case is equivalent to the exponential distribution discussed in the previous paragraph. The transfer function is given by

$$\tau(\omega) \approx d_0 \rho_0 \sqrt{\frac{\pi}{4a + 2jw}}. \tag{10}$$

The Gaussian distribution for the cluster of scatterers centered at the origin of the coordinate system readily suggests a model for the case where the cluster is centered at any other point, e.g., over the ellipse of "modulus" μ_0: $\bar{\rho}(\mu) = \rho_0 \exp[-a(\mu - \mu_0)^2]$.[1] The transfer function turns out to be

$$\tau(\omega) \approx d_0 \rho_0 \sqrt{\frac{\pi}{4a + 2jw}}\, \mathcal{E}\left(\frac{a\mu_0}{\sqrt{a + \frac{jw}{2}}}\right) e^{-j\frac{a\mu_0^2 w}{2a + jw}} \tag{11}$$

where $\mathcal{E}(z) = 1 + \mathrm{erf}(z)$, and $\mathrm{erf}(z)$ is the error function [10]. Fig. 3 shows this approximation for $\tau(\omega)$, for a cluster centered at $\mu_0 = 0.5$ and three widths. For the largest width ($a = 1$) and $w \gtrsim 10$, $|\tau(\omega)|$ is dominated by the $\omega^{-1/2}$ decay, while $\arg \tau(\omega) \approx -\pi/4$. As the cluster shrinks (i.e., as a grows), $|\tau(\omega)|$ develops a plateau at low frequencies, which shifts toward the right as a becomes larger. Meanwhile, the range of variation of $\arg \tau(\omega)$ widens and, for $a = 100$, it winds a few times around the interval $(-\pi, \pi)$. In this way, the transfer function for the cluster approaches the limit of a point scatterer, i.e., $\rho(\mathbf{r}) \sim \delta(\mathbf{r} - \mathbf{r}_0)$, with $\delta(\mathbf{r})$ the Dirac delta function, for which $\bar{\rho}(\mu) = \rho_0 \delta(\mu - \mu_0)$. At the limit, the (exact) transfer function is $\tau(\omega) = d_0 \rho_0 \exp[jw(1 - \cosh \mu_0)]$, and thus, $|\tau(\omega)|$ is a constant, and $\arg \tau(\omega)$ is proportional to the frequency.

[1]Note that, in contrast with all the cases considered earlier, in this form of $\bar{\rho}(\mu)$ the coefficient ρ_0 does not stand for the scatterer density at $\mu = 0$, as in the other cases, but at the distribution maximum ($\mu = \mu_0$).

III. Numerical Simulations

In order to compare our analytical calculation of $\tau(\omega)$ with a more realistic representation of the scattering channel, we have evaluated the transfer function by simulating the transmission of a real-life signal through an ensemble of point scatterers with different cross sections. We consider $N = 10^6$ scatterers, randomly distributed over the plane, following a prescribed probability density $\bar{\rho}(\mu)$. Their cross sections are chosen in such a way that the square roots $\sqrt{\sigma_k}$ are uniformly distributed between 0 and 2 m, with their mean value thus being $\langle \sqrt{\sigma} \rangle = 1$ m. The distance between the emitter and the receiver is $d_0 = 10^4$ m.

To build up a surrogate of the emitter signal, i.e., $E(t)$ in (1), we have acquired a 1-s-long sample of the signal detected by a DVB−T+DAB+FM dongle (RTL2832U+R820T) connected to a MacBook Pro. The sampling frequency was 2 MHz, with a resulting bandwidth of 1 MHz. The signal was measured around 102.5 MHz, which corresponds to the frequency of one of the local FM radio stations. The 8-bit digitalized I- and Q-channel outputs were combined by the computer into a single real number, given by the modulus of the corresponding complex signal. Simulations were performed using the first 2^{16} points in the signal.

For numerical treatment, not only $E(t)$ but also the receiver signal $R(t)$ must be discretized in time. A convenient form to rewrite (1), taking into account this discretization, is given by

$$R[s] = \frac{1}{d_0} E[s - s_0] + \sum_{k=1}^{N} \frac{\sqrt{\sigma_k}}{d_E^{(k)} d_R^{(k)}} E[s - s_k] \tag{12}$$

where the integer index s replaces the continuous time variable. The delays in s are now given by $s_0 = \lfloor d_0/c\delta t \rfloor$ and $s_k = \lfloor (d_E^{(k)} + d_R^{(k)})/c\delta t \rfloor$, where $\lfloor \cdot \rfloor$ indicates the floor function (largest lower integer), and $\delta t = 0.5 \times 10^{-6}$ s is the sampling time. We assume, moreover, that $E[s] = 0$, for $s < 0$. To calculate the transfer function from (2), the Fourier transforms of $E(t)$ and $R(t)$ are computed through a standard fast Fourier transform algorithm implemented in MATLAB, and their ratio is evaluated for each value of the frequency ω.

Dots in Fig. 4 show our simulation results on a Bode diagram for two forms of $\bar{\rho}(\mu)$, while curves stand for the corresponding analytical results. For clarity in the graphical representation of the numerical data, only about 2000 points out of the 2^{15} calculated values for $\tau(\omega)$ have been plotted. We find that, except for a sizable difference for large frequencies, which is discussed in the next paragraph, the agreement between numerical and analytical results is excellent. Even for the Gaussian distribution (see case (b) in Fig. 4), for which the analytical result of (11) has been obtained within the approximation of large frequencies, the coincidence spans both small and large values of w, until the results begin to diverge noticeably for $w \gtrsim 50$ to 100.

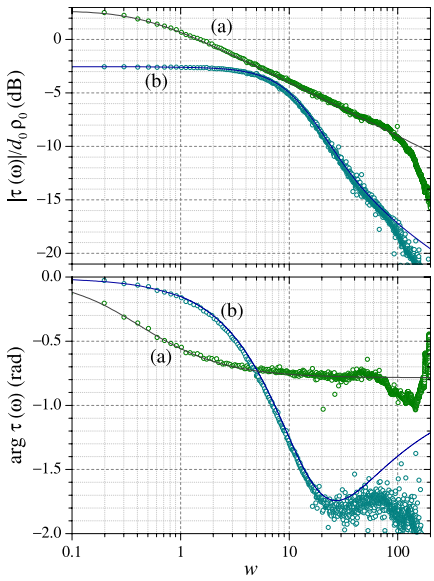

Fig. 4. Dots represent the transfer function calculated from numerical simulations for 10^6 point scatterers distributed according to (a) the exponential $\bar{\rho}(\mu) = \rho_0 \exp[\alpha(1 - \cosh \mu)]$ with $\alpha = 0.3$, and (b) the Gaussian $\bar{\rho}(\mu) = \rho_0 \exp[-a(\mu - \mu_0)^2]$ with $a = 10$ and $\mu_0 = 0.5$. Curves stand for the corresponding analytical results. Note that the axes scales differ from those in Figs. 2 and 3.

It turns out that the difference between analytical and numerical results for large frequencies is a consequence of the time discretization of the signals in the simulation. Discretization of the receiver signal, in particular, amounts to the impossibility to discern between scatterers for which the delays T_k in (1) differ by less than the sampling time δt. This impossibility is inconsequential for small frequencies, where all scatterers contribute to $\tau(\omega)$ with similar weights, but becomes crucial for large ω, where the transfer function is strongly dominated by the scatterers situated close to the line that joins the emitter and the receiver (i.e., with small μ; see Section II-B). An approximate mathematical representation of this effect is to transform the integral in (4) into a summation over discrete values of μ, corresponding to the successive distance intervals within which time delays cannot be discerned from each other. Results of this procedure, which we do not present here, show that, in fact, the $w^{-1/2}$-decay of the analytical transfer function is replaced, for sufficiently large w, by an exponential cutoff. This cutoff is here an artifact of the time discretization in numerical simulations. However, it could in practice modify the transfer function, if $\tau(\omega)$ included the contribution not only of the scatterers but also of an actual digitalization of the signal by the emitter and/or the receiver.

IV. Conclusion

Modeling of the environment as a transmission channel for radar signals is based on an educated guess on the various factors that modify electromagnetic radiation from emission to reception. Among these factors, the spatial distribution of scatterers (each of them endowed with its respective scattering cross section) determines the collection of echoes that build up the received signal. In this letter, we have presented analytical results on the transfer function for a series of planar distributions of stationary scatterers in a bistatic configuration, i.e., with noncollocated emitter and receiver. In contrast with common statistical models of environment radar cross sections [7], [8], the transfer function bears information on the signal phase and its modification along transmission (due to the echoes' time delays), and it is therefore not limited to the quantification of the power transfer by incoherent signals. On the other hand, our results disregard possible effects of radiation polarization.

The key assumption that the scattering cross section is continuously distributed over the plane, around the emitter and the receiver, makes it possible to obtain explicit mathematical expressions for the transfer function. For some specific distributions, these expressions are exact, and systematic approximations can be obtained for more general cases. In all situations, they reveal the low-pass-filter nature of the environment as a transmission channel. It is also worthwhile pointing out that the inverse problem, i.e., inferring the scatterers' distribution from the transfer function, can be addressed by means of the same formulation. Numerical simulations of the transmission process, using a discrete distribution of point scatterers and a real-life radio signal, generally validate the analytical results and, at the same time, disclose possible deviations and their origin.

Finally, we remark that our mathematical approach may be employed in the calculation of transfer functions for scatterer distributions with stochastic components. Work is in progress along this line. With suitable adaptations, moreover, the method could also be useful in the computation of a series of quantities relevant to radar signal propagation and related problems. Examples are autocorrelation, cross-correlation, and ambiguity functions; power spectral densities; and signal models with moving emitter and/or receiver [5], [7], [8].

Acknowledgment

The authors would like to thank Dr. M. Magaña, from the School of Electrical Engineering and Computer Science of Oregon State University, and Dr. A. Roncagliolo, from Universidad Nacional de La Plata, for their critical reading of the manuscript.

References

[1] N. J. Willis and H. D. Griffiths, *Advances in Bistatic Radar*. Raleigh, NC, USA: SciTech Publ., 2007.
[2] W. A. Qazi, W. J. Emery, and B. Fox-Kemper, "Computing ocean surface currents over the coastal California current system using 30-min-lag sequential SAR Images," *IEEE Trans. Geosci. Remote Sens.*, vol. 52, no. 12, pp. 7559–7580, Dec. 2014.
[3] R. Iglesias *et al.*, "Ground-based polarimetric SAR interferometry for the monitoring of terrain displacement," *IEEE J. Sel. Top. Appl. Earth Obs.*, vol. 8, no. 3, pp. 980–993, Mar. 2015.
[4] A. Monti Guarnieri, A. Broquetas, A. Recchia, and F. Rocca, and J. Ruiz-Rodon, "Advanced radar geosynchronous observation system: ARGOS," *IEEE Geosci. Remote Sens. Lett.*, vol. 12, no. 7, pp. 1406–1410, Jul. 2015.
[5] I. Walterscheid, J. H. G. Ender, A. R. Brenner, and O. Loffeld, "Bistatic SAR processing and experiments," *IEEE Trans. Geosci. Remote Sens.*, vol. 44, no. 10, pp. 2710–2717, Oct. 2006.
[6] P. E. Howland, D. Maksimiuk, and G. Reitsma, "FM radio based bistatic radar," *Proc. Inst. Elect. Eng.—Radar Sonar Navig.*, vol. 152, no. 3, pp. 107–115, Jun. 2005.
[7] M. A. Richards, *Fundamentals of Radar Signal Processing*. New York, NY, USA: McGraw-Hill, 2005.
[8] A. Goldsmith, *Wireless Communications*. Cambridge, U.K.: Cambridge Univ. Press, 2005.
[9] G. Woan, *The Cambridge Handbook of Physics Formulas*. Cambridge, U.K.: Cambridge Univ. Press, 2010.
[10] F. W. J. Olver, D. W. Lozier, R. F. Boisvert, and Ch. W. Clark, *NIST Handbook of Mathematical Functions*. Cambridge, U.K.: Cambridge Univ. Press, 2010. [Online]. Available: http://dlmf.nist.gov